Available online at www.sciencedirect.com
ScienceDirect
Journal of the European Ceramic Society 29 (2009) 1449–1455
www.elsevier.com/locate/jeurceramsoc

Microstructural, structural and dielectric properties of Er^{3+}-modified $BaTi_{0.85}Zr_{0.15}O_3$ ceramics

E. Antonelli, M. Letonturier, J.-C. M'Peko *, A.C. Hernandes

Grupo de Crescimento de Cristais e Materiais Cerâmicos, Instituto de Física de São Carlos (IFSC), Universidade de São Paulo (USP), C. Postal: 369, CEP: 13560-970 São Carlos/SP, Brazil

Received 17 March 2008; received in revised form 3 September 2008; accepted 13 September 2008
Available online 5 November 2008

Abstract

The (micro)structural and electrical properties of undoped and Er^{3+}-doped $BaTi_{0.85}Zr_{0.15}O_3$ ceramics were studied in this work for both nominal Ba^{2+} and Ti^{4+} substitution formulations. The ceramics were produced from solid-state reaction and sintered at 1400 °C for 3 h. For those materials prepared following the donor-type nominal $Ba_{1-x}Er_x(Ti_{0.85}Zr_{0.15})O_3$ composition, especially, Er^{3+} however showed a preferential substitution for the $(Ti,Zr)^{4+}$ lattice sites. This allowed synthesis of a finally acceptor-like, highly resistive $Ba(Ti,Zr,Er)O_{3-\delta}$-like system, with a solubility limit below but close to 3 cat.% Er^{3+}. The overall phase development is discussed in terms of the amphoteric nature of Er^{3+}, and appears to mainly or, at least, partially also involve a minimization of stress effects from the ion size mismatch between the dopant and host cations. Further results presented here include a comparative analysis of the behavior of the materials' grain size, electrical properties and nature of the ferroelectric-to-paraelectric phase transition upon variation of the formulation and Er^{3+} content.

Keywords: Sintering; Microstructure-final; Electrical properties; Ferroelectric properties; $BaTiO_3$ and titanates

1. Introduction

The study of ABO_3-type solid solutions based on perovskite-structured barium titanate ($BaTiO_3$) has so far been of great interest as it offers the possibility to optimize several electrical properties for the manufacture of a number of devices, including multilayer capacitors.[1] In particular, $BaTi_{1-x}Zr_xO_3$ materials have been explored, showing that, in appropriate amounts, Zr^{4+} induces an increase of the dielectric constant, tunability under biasing field and a reduction of the low-frequency dielectric losses.[2–4] On the other hand, the addition of rare-earth (R^{3+}) elements to $BaTiO_3$ has been considered also for producing semiconducting materials that enable the development of positive temperature coefficient resistors.[1] Of special interest for the present work is the fact that some rare-earth cations reveal an amphoteric behavior when being incorporated into the $BaTiO_3$ structure. That is, lanthanide ions from Sm^{3+} to Er^{3+} with intermediate size between Ba^{2+} and Ti^{4+} can be accommodated at any of both the A or B lattice sites, depending on doping concentration and stoichiometry of the hosting $BaTiO_3$ structure.[5–7] For such cations, in practice, the following two possible single site-substitution procedures of material preparation may be formulated:

$$(1-x)BaO + xRO_{1.5} + TiO_2 \rightarrow Ba_{1-x}R_xTiO_3, \quad (1.1)$$

$$BaO + (1-x)TiO_2 + xRO_{1.5} \rightarrow BaTi_{1-x}R_xO_{3-x/2}, \quad (1.2)$$

according to which R^{3+} is planed to incorporate at the Ba^{2+} or Ti^{4+} sites, respectively. The proposed incorporation reactions, with their respective compensating mechanisms, that may develop in these cases are (Kröger-Vink notation)[6]:

$$R_2O_3 + 2TiO_2 \rightarrow 2R_{Ba}^{\bullet} + 2Ti_{Ti}^{x} + 6O_O^x + \tfrac{1}{2}O_2 + 2e', \quad (2.1)$$

$$R_2O_3 + 3TiO_2 \rightarrow 2R_{Ba}^{\bullet} + 3Ti_{Ti}^{x} + 9O_O^x + V_{Ba}'', \quad (2.2)$$

$$2R_2O_3 + 3TiO_2 \rightarrow 4R_{Ba}^{\bullet} + 3Ti_{Ti}^{x} + 12O_O^x + V_{Ti}'''', \quad (2.3)$$

$$2BaO + R_2O_3 \rightarrow 2Ba_{Ba}^{x} + 2R_{Ti}' + 5O_O^x + V_O^{\bullet\bullet}, \quad (2.4)$$

$$R_2O_3 \rightarrow R_{Ba}^{\bullet} + R_{Ti}' + 3O_O^x. \quad (2.5)$$

* Corresponding author. Fax: +55 16 33739824.
E-mail address: peko@if.sc.usp.br (J.-C. M'Peko).

0955-2219/$ – see front matter © 2008 Elsevier Ltd. All rights reserved.
doi:10.1016/j.jeurceramsoc.2008.09.009

On one hand, according to the reaction (2.1), substitution of R^{3+} for Ba^{2+} may yield $R_{Ba}^{\bullet}$ with extra electrons as compensating defects, the material resulting a donor-type semiconductor with the above final $Ba_{1-x}R_xTiO_3$ formula interpreted as $Ba_{1-x}{}^{2+}R_x{}^{3+}Ti_{1-x}{}^{4+}Ti_x{}^{3+}O_3{}^{2-}$, where $Ti^{3+} \equiv (Ti^{4+}\ e')$. On the other hand, according to the reactions (2.2)–(2.4), substitution of R^{3+} for Ba^{2+} or Ti^{4+} yields $R_{Ba}^{\bullet}$ or R'_{Ti} with, respectively, compensating Ba^{2+}, Ti^{4+} or O^{2-} vacancies (V''_{Ba}, V''''_{Ti} or $V_O^{\bullet\bullet}$) defects, and the acceptor-doped material so obtained is expected to basically result insulator in nature. The reaction (2.5) refers to a simultaneous incorporation of the dopant at both the Ba^{2+} and Ti^{4+} sites with self compensation.

In terms of resulting stoichiometry, however, the experimental results so far collected in literature often depart noticeably from considering development of only one of the above reaction predictions. That is, for instance, for samples prepared so as to produce a $Ba_{1-x}Er_xTiO_3$ composition, one observes that, with increasing Er^{3+}, the materials change from insulators (high electrical resistivity for $x=0$) to semiconductors (low electrical resistivity), as expected for the reaction (2.1), but gradually recover however an insulating nature towards higher Er^{3+} content.[5,6] This result suggests a change of compensating mechanism and, thus, a need of also considering reactions (2.2)–(2.5), when the dopant content exceeds a given value. Indeed, data processed from applying different techniques that include X-ray diffraction and electrical measurements support the idea that, in Er^{3+}-doped $BaTiO_3$, incorporation of the dopant appears to instead occur at both cation sites, irrespective of an obvious preference for either the Ba^{2+} or Ti^{4+} sites, depending on doping concentration and stoichiometry of the hosting material.[5–7] In other words, incorporation of Er^{3+} at any of both host cation sites in $BaTiO_3$ should not be totally ruled out without previously carrying out a careful data analysis. From the structural viewpoint, moreover, prepared $Ba_{1-x}Er_xTiO_3$ samples have shown to be single-phase compounds below $x=0.01$, while an additional $Er_2Ti_2O_7$ pyroclore-like phase appears above.[6] When the samples are prepared so as to produce the $BaTi_{1-x}Er_xO_{3-x/2}$ formula, the composition range of single-phase compounds noticeably increases.[6] These and others results[5–7] have allowed inference that the solubility limit of Er^{3+} in the Ba^{2+} sites remains below $x=0.01$, while locating above this value (apparently in the $0.08 \leq x \leq 0.1$ composition range) for substitution at the Ti^{4+} lattice sites.

Although the influence of rare-earth elements on the dielectric properties of $BaTiO_3$ has been widely investigated, the literature recognizes, however, that works dealing with rare-earth dopants in, for instance, $Ba(Ti,Zr)O_3$ ceramics are indeed scarce.[8,9] In the present work, the possibility of synthesizing Er^{3+} and Zr^{4+} co-doped $BaTiO_3$ materials, with the nominal $Ba_{1-x}Er_x(Ti,Zr)O_3$ formula, was explored. The results here presented and discussed refer to the trend of phase development induced by Er^{3+} in the presence of Zr^{4+}, most probable crystallographic occupation site for Er^{3+}, thermal spectra of permittivity and resulting behaviors of the permittivity and ferroelectric-to-paraelectric transition phase upon variation of the rare-earth dopant content. For an appropriate comparison, moreover, some samples with the nominal $Ba(Ti_{1-x}Er_x,Zr)O_{3-x/2}$ formula were also prepared and studied.

2. Experimental procedure

The studied materials were prepared through the conventional ceramic method, starting from high-purity precursor powders of $BaCO_3$ (Riedel, 99%), TiO_2 (Strem Chemicals, 99.5%), ZrO_2 (Alfa Aesar, 99%) and Er_2O_3 (Alfa Aesar, 99.9%). These raw materials were mixed in stoichiometric proportions according to the nominal formulation:

$$(1-x)BaO + xErO_{1.5} + 0.85TiO_2 + 0.15ZrO_2 \rightarrow Ba_{1-x}Er_x(Ti_{0.85}Zr_{0.15})O_3, \quad (3)$$

where $x=0$, 0.005, 0.03 and 0.30, hereafter labeled as BTZ15, (BE)TZ005, (BE)TZ03, (BE)TZ30, respectively. To complete our study, in addition, some samples with the nominal formulation:

$$BaO + (0.85-x)TiO_2 + xErO_{1.5} + 0.15ZrO_2 \rightarrow Ba(Ti_{0.85-x}Er_xZr_{0.15})O_{3-x/2}, \quad (4)$$

were prepared, with $x=0.005$ and 0.03, hereafter denoted as B(TE)Z005 and B(TE)Z03, respectively. After homogenization for 24 h, the mixtures were calcined at 1200 °C for 2 h, ball-milled for 12 h into fine powders, compacted into disk-shaped samples and then sintered at 1400 °C for 3 h. The final density of each sintered specimen was determined by the Archimedes method, showing values above 95% of the $BaTiO_3$'s theoretical density in all cases. On the other hand, both Er^{3+}-modified phase and microstructure developments were followed by X-ray diffraction (XRD) using a Rigaku Geigerflex diffractometer (with a monochromatic Cu Kα radiation, $\lambda = 1.5406$ Å) and scanning electron microscopy (SEM) using a Zeiss DSM-960 equipment, respectively. The latter was fitted with fully automated equipment for quantitative energy-dispersive X-ray spectroscopy (EDS) analysis. Grain size of the ceramics was evaluated by the intercept method directly on the SEM images. Electrical measurements were carried out with a Solartron SI 1260 impedance/gain-phase analyzer over a wide temperature range from −150 to 200 °C and frequency range from 100 Hz to 1 MHz. Electric contacts consisted of platinum (Pt) paste previously applied on both parallel faces of the pellets and diffused at 700 °C for 1 h.

3. Results and discussion

As an example, Fig. 1 shows the XRD patterns corresponding to the BTZ15 and (BE)TZ005 powders after calcination (at 1200 °C for 2 h). A direct comparison between the two spectra allows to discuss on the trend of phase development in both undoped and Er^{3+}-containing $Ba(Ti,Zr)O_3$ systems. That is, Fig. 1a reflects the formation of a single-phase compound that was identified to be isostructural with the cubic $BaTi_{0.75}Zr_{0.25}O_3$ (BTZ25) phase. Accordingly, the formation of the starting BTZ15 phase may be assumed with a pseudo-cubic

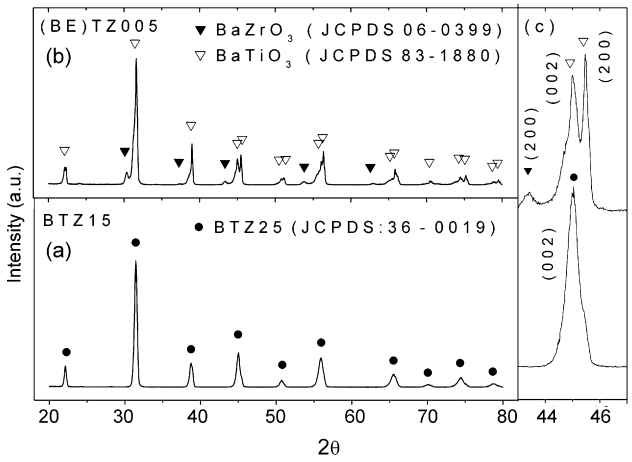

Fig. 1. X-ray diffraction patterns of the (a) BTZ15 and (b) (BE)TZ005 powders calcined at 1200 °C for 2 h. (c) is a magnification of these patterns around $2\theta = 45°$.

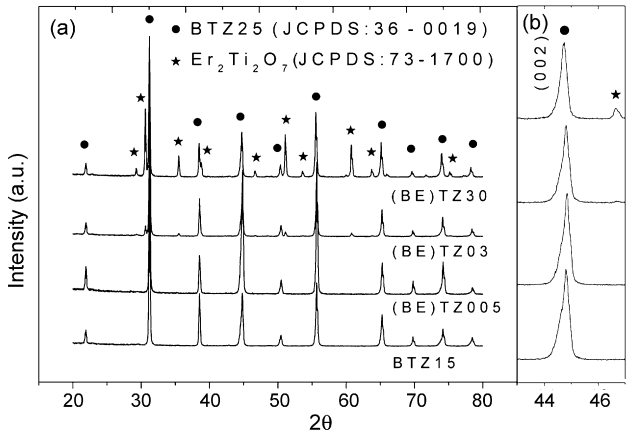

Fig. 2. X-ray diffraction patterns of the (a) BTZ15, (BE)TZ005, (BE)TZ03 and (BE)TZ30 ceramics sintered at 1400 °C for 3 h. (b) is a magnification of these patterns around $2\theta = 45°$.

symmetry. Meanwhile, Fig. 1b indicates the formation of two distinct phases that were identified to be isostructural with the tetragonal $BaTiO_3$, as major phase, and the cubic $BaZrO_3$, as minor phase. As no $BaZrO_3$ formed in the undoped BTZ15 system prepared, the conclusion is that, during thermal treatment, addition of Er^{3+} promoted the formation of a $Ba(Zr,Er)O_{3-\delta}$ phase while leaving free of Er^{3+} a $BaTiO_3$-based phase, which is of high tetragonality at room temperature, when highly to totally pure. Fig. 1c is a magnification of the diffraction spectra around $2\theta = 45°$, showing a cubic-like, single reflection peak (0 0 2) for BTZ15 and its clear split into the reflection peaks (0 0 2) and (2 0 0) for an expected highly pure and, thus, high-tetragonality $BaTiO_3$ phase. To further understanding the above phase development trend, the values of ionic radii (IR) of the involved cations should be compared. Considering the twelve- and six-coordination numbers (CN) holding, respectively, for the A and B sites in the perovskite ABO_3 structure, these values are 1.61 Å for Ba^{2+}, 0.605 Å for Ti^{4+}, 0.72 Å for Zr^{4+} and 1.00 or 0.89 Å for Er^{3+} if substituting, respectively, for the A or B sites.[10] In terms of absolute values, the involved degree of ionic radius mismatch are $\Delta IR(Er - Ba) = 0.61$ Å, $\Delta IR(Er - Ti) = 0.28$ Å, $\Delta IR(Er - Zr) = 0.17$ Å. In other words, substitution of Er^{3+} for Zr^{4+} is expected to involve stress effects relatively to considerably lower than the substitution for either Ti^{4+} or Ba^{2+}. This fact should account for the formation trend of, separately, $BaTiO_3$ and $Ba(Zr,Er)O_{3-\delta}$ in Er^{3+} and Zr^{4+} co-doped $BaTiO_3$ materials in the early stage of oxides reaction during thermal treatment (in this case, at the calcination conditions applied: 1200 °C for 2 h).

Fig. 2a now shows the XRD patterns of the prepared undoped BTZ15 and (BE)TZ samples after sintering (at 1400 °C for 3 h). As compared to Fig. 1, both BTZ15 and (BE)TZ005 samples actually show to be single-phase compounds. This result suggests that the two $BaTiO_3$ and $Ba(Zr,Er)O_{3-\delta}$ compounds, as initially detected in the calcined (BE)TZ005 powder (Fig. 1b), reacted to finally give either a $(Ba,Er)(Ti,Zr)O_3$ or $Ba(Ti,Zr,Er)O_{3-\delta}$-type phase, the proper compound of which will be discriminated below. Fig. 2b is a magnification of all the diffraction spectra around $2\theta = 45°$. The poor split of the reflection peak (0 0 2) observed in all the spectra suggests the formation of pseudo-cubic phases for all these prepared samples. For (BE)TZ03 and (BE)TZ30, moreover, the XRD spectra of Fig. 2 show the formation of an additional phase that was identified to be isostructural with the pyroclore $Er_2Ti_2O_7$. This and other observations (discussed later) suggest that, with increasing its concentration, the solubility limit of Er^{3+} into $Ba(Ti_{0.85}Zr_{0.15})O_3$ should locate close to $x = 0.03$ (3 at.%) when the materials are nominally formulated so as Er^{3+} to substitute for Ba^{2+}. An important fact to point out is that all these sintered samples showed to be extremely insulators, with room-temperature resistivity values ranging beyond 10^{10} Ω cm. This result seemingly rules out any attempt to propose real substitution of Ba^{2+} by Er^{3+} for these (BE)TZ formulated materials, that is, even for the $x = 0.005$ composition, *i.e.* the (BE)TZ005 sample, for which a strong or, at least, moderate semiconducting behavior would be expected in a Zr^{4+}-free $(Ba,Er)TiO_3$ system.[5,6] In other words, irrespective of the donor-type nominal composition formulated, substitution of Er^{3+} should rather occur at the $(Ti,Zr)^{4+}$ sites, the materials' stoichiometry thus behaving like that expected from the acceptor-type formulation (1.2). In R^{3+}-doped $BaTiO_3$, substitution of amphoteric R^{3+} cations for either Ba^{2+} or Ti^{4+} has been often argued to depend on the Ba/Ti ($\equiv\Gamma$) ratio: that is, $\Gamma < 1$ and $\Gamma > 1$, respectively.[5–7] Accordingly, the value of $\Gamma > 1$ applying in our Er^{3+}-doped $Ba(Ti_{0.85}Zr_{0.15})O_3$ system would presuppose the substitution of Er^{3+} at the $(Ti,Zr)^{4+}$ lattice sites. We however note that, besides the fact that the above Ba/Ti ratio criteria agree with experiment only over restricted compositions range (as was already discussed in Section 1), verification or not of a full validity of such criteria appears to still need fulfillment of further specific works devoted to closely treat this question in originally doped and co-doped $BaTiO_3$ systems, *i.e.* compounds of the type $(A',A'')(B',B'')O_3 = (Ba,A'')(Ti,B'')O_3$ doped with amphoteric R^{3+} cations. In any case, the selective incorporation tendency of Er^{3+} at finally the $(Ti,Zr)^{4+}$ lattice sites appears to mainly or, at least, partially also originate, in this work, as a consequence of the features of phase development when introducing Er^{3+} into

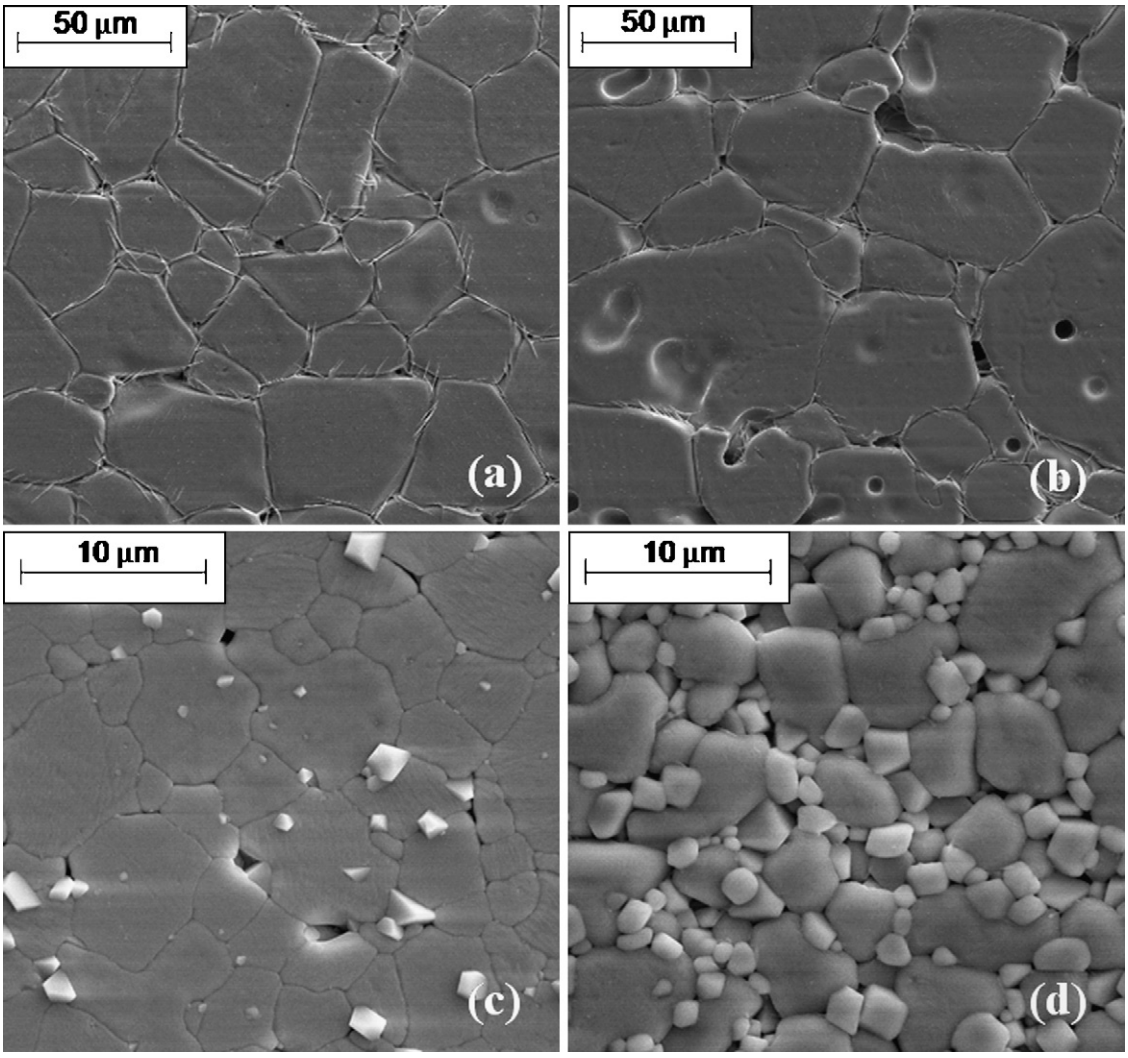

Fig. 3. SEM micrographs of (a) BTZ15, (b) (BE)TZ005, (c) (BE)TZ03 and (BE)TZ30 polished and thermally etched samples.

the $BaTiO_3$ structure in the presence of Zr^{4+}. As was discussed above with respect to Fig. 1, the stress energy effects associated with the ion size mismatch between the dopant and host cations in Er^{3+} and Zr^{4+} co-doped $BaTiO_3$ ceramics appear to favor substitution of Er^{3+} for Zr^{4+}, allowing the formation of initially $BaTiO_3$ and $Ba(Zr,Er)O_{3-\delta}$ during calcination. As the temperature is further increased (during sintering), these intermediary compounds subsequently react so as to finally give an insulating $Ba(Ti,Zr,Er)O_{3-\delta}$-like compound.

Fig. 3 shows the SEM micrographs corresponding to these undoped BTZ15 and (BE)TZ samples after sintering, polishing and thermal etching. The microstructures from the BTZ15 and (BE)TZ005 samples (Fig. 3a and b) consist of large grains, that revealed an average size of about 29 μm, surrounded by a modest intergranular thin layer that was identified to be a Ti^{4+}-rich phase, according to the EDS analysis performed (that gave Ba/Ti ratios of 0.8 and 0.9, respectively, *versus* 1.4 and 1.3 for the grain phase). This suggests the formation of a Ti^{4+}-induced intergranular liquid phase during the materials' sintering process, as it often happens in $BaTiO_3$-based ceramics treated at temperatures above about 1300 °C.[11] The liquid phase normally enhances mass transport between grains, promoting thus a grain growth process. For the (BE)TZ03 and (BE)TZ30 samples (Fig. 3c and d), no clear evidence of liquid phase formation was observed, while the materials' grain size drastically reduced to an average value of about 4 μm, indicating that presence of Er^{3+} acts as a grain growth inhibitor factor in $BaTiO_3$ ceramics, in good agreement with previous literature.[6,7] In these two cases, moreover, the microstructures show the presence of a second phase characterized by small brighter grains, with an average grain size of about 1.5 μm. Besides containing Ba^{2+} and Zr^{4+} elements in few amounts, these grains were identified to be rich in Er^{3+} followed by Ti^{4+}, according to the EDS analysis (that gave an apparent Er/Ti ratio of about 1.3 in both cases), and should indeed represent the $Er_2Ti_2O_7$ phase, as identified from the XRD analysis (Fig. 2). The very low concentration of this second phase in the (BE)TZ03 sample (Fig. 3c) suggests that this composition ($x = 0.03$) locates above but relatively close to the solubility limit of Er^{3+} into $Ba(Ti,Zr,Er)O_{3-\delta}$, a result on which we will be back below in terms of apparent (direct or indirectly) driving force.

To complete and further understanding the peculiarities of phase formation when introducing Er^{3+} into the $Ba(Ti,Zr)O_3$

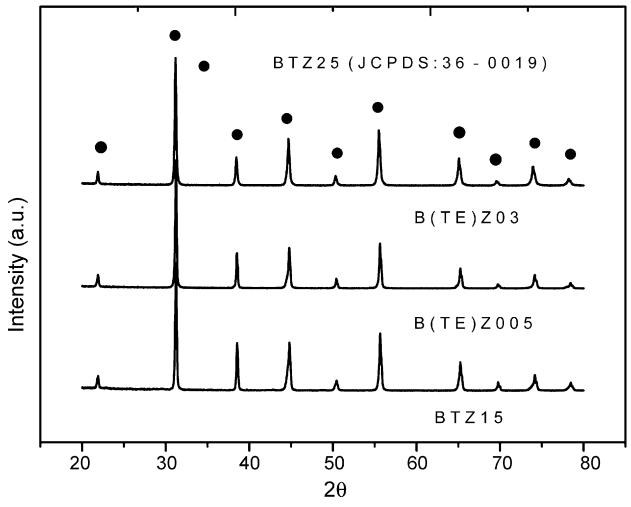

Fig. 4. X-ray diffraction patterns of the BTZ15, B(TE)Z005 and B(TE)Z30 ceramics sintered at 1400 °C for 3 h.

system, Figs. 4 and 5 show, respectively, the XRD patterns and the SEM micrographs corresponding to the sintered materials prepared according to the formulation (4), *i.e.* B(TE)Z005 and B(TE)Z03. For these samples, only the formation of single-phase compounds was detected, with reflection peaks also isostructural with BTZ25 (Fig. 4). On the other hand, the samples' microstructures reveal grains with an average size of 8 and 5 μm, respectively, for both B(TE)Z005 and B(TE)Z03 materials (Fig. 5). When compared to the (BE)TZ005 sample, for which an average grain size of 29 μm was found (Fig. 3), the drastic reduction of grain size for the B(TE)Z005 sample (8 μm) should be accounted for the non-formation of intergranular liquid phase, during the material sintering process, as a result of Ti^{4+} reduction in the system. In the context of the present work, what is quite important to highlight is that, for these B(TE)Z samples, no second phase was found, that is, even for $x = 0.03$. This result contrasts with that obtained for the formulation (3), but remains in good agreement with literature where, as mentioned above, the solubility limit of Er^{3+} at the Ti^{4+} sites in Er^{3+}-doped $BaTiO_3$ compounds apparently locates in the $0.08 \leq x \leq 0.1$ composition range.[5–7] Consequently, the solubility limit locating close to $x = 0.03$ and subsequent formation of a $Er_2Ti_2O_7$ second phase, as found for the (BE)TZ formulated system, should be (direct or indirectly) promoted by the introduction of Ba^{2+} vacancies, as this system is prepared so as Er^{3+} to substitute for Ba^{2+} (*i.e.*, $x\,Er^{3+}$ in place of $x\,V''_{Ba}$ in the nominally formulated $Ba_{1-x}Er_xTi_{0.85}Zr_{0.15}$ compounds), while in practice Er^{3+} incorporates with a rather preference for the $(Ti,Zr)^{4+}$ sites (*i.e.*, synthesis of an apparently $Ba_{1-x}(V_{Ba})_x(Ti,Zr,Er)O_{3-\delta}$-like system, to be or not however confirmed only after the fulfillment of specific works devoted to closely treat this complicated stoichiometry question).

Fig. 6a shows the temperature dependence of permittivity measured at the frequency of 1 kHz for all the sintered (BE)TZ formulated materials. The dielectric spectra are characterized by dielectric peaks that correspond to the expected ferroelectric-to-paraelectric phase transitions. In addition, the nature of this transition is seen to change from normal (sharp-like dielectric peak) to diffuse (broad-like dielectric peak) when the Er^{3+} content increases. On the other hand, Fig. 6b illustrates, just as an example, the temperature dependence of permittivity recorded at various frequencies for BTZ15 and (BE)TZ30. Also, a change from normal (frequency independent) to relaxor (frequency dependent) phase transition develops when increasing the Er^{3+} content. Quantitatively speaking, the diffuseness of the phase transition might be described by an empirical parameter ΔT_{dif} that can be defined as $\Delta T_{dif} = T_{0.9\varepsilon m} - T_m$,[12] where $T_{0.9\varepsilon m}$ and T_m represent, respectively, the temperature corresponding to 90% of the maximum permittivity (ε_m) at the right peak side and the temperature at ε_m, both according to measurements conducted at 1 kHz, for instance. On the other hand, the materials' relaxor behavior around the phase transition might be in turn described by an empirical parameter ΔT_{relax} that can be defined as $\Delta T_{relax} = T_m\ (100\,Hz) - T_m\ (100\,kHz)$.[12] Fig. 7 summarizes the behavior of these parameters upon variation of the Er^{3+} content for both (BE)TZ and B(TE)Z formulated systems, while Fig. 8 refers to the behaviors corresponding to the

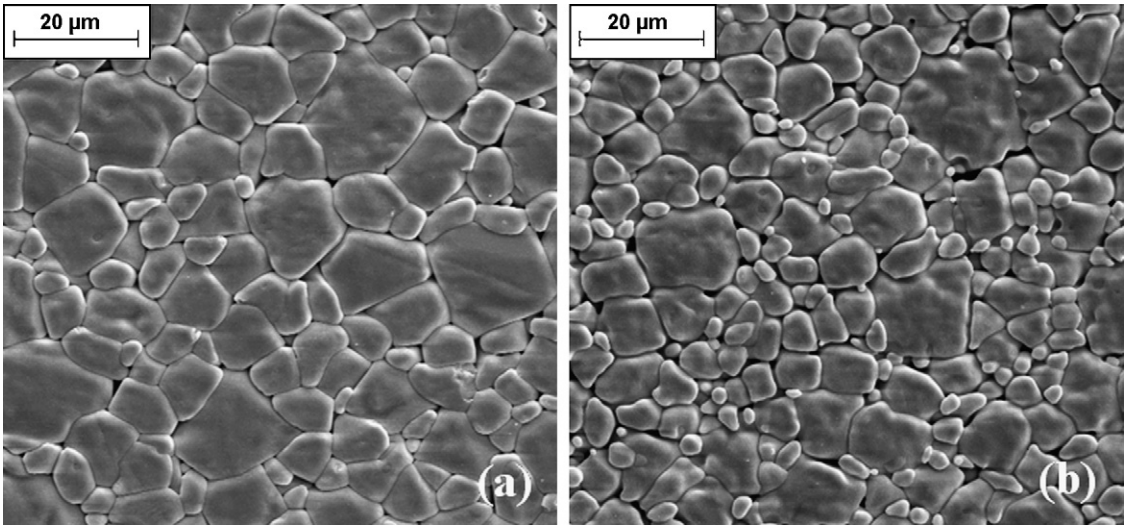

Fig. 5. SEM micrographs of (a) B(TE)Z005 and (b) B(TE)Z30 polished and thermally etched samples.

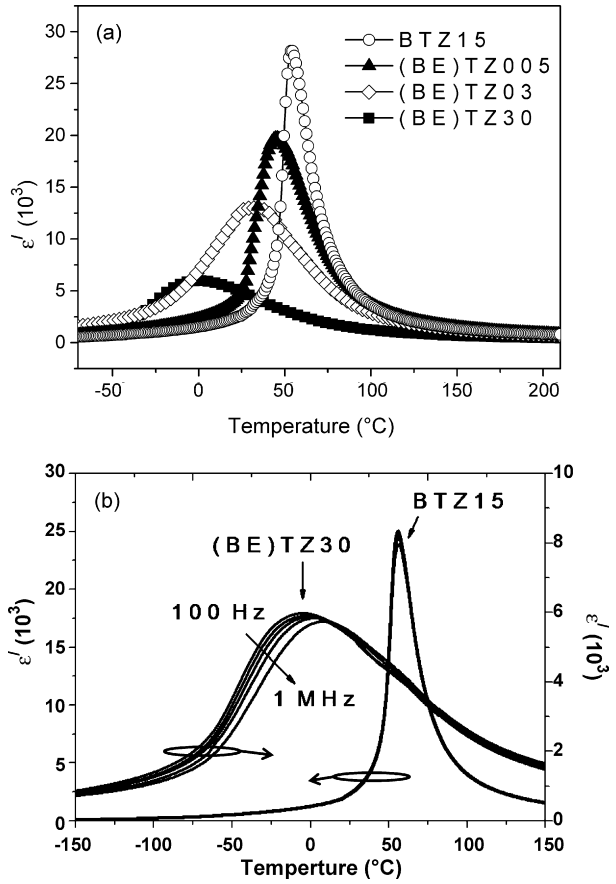

Fig. 6. Temperature dependence of permittivity (ε) for (a) all the sintered (BE)TZ samples, according to electrical measurements conducted at 1 kHz, and (b) BTZ15 (left scale) and (BE)TZ30 (rifgt scale) at various frequencies: 10^2, 10^3, 10^4, 10^5, 10^6 Hz (in the direction of the arrow).

maximum permittivity (ε_m) and phase transition temperature (T_m) processed from the 1 kHz-electrical data. For the B(TE)Z system, over the $0 \le x \le 0.03$ composition range studied, the materials' ΔT_{dif} and ΔT_{relax} parameters increase continuously with increasing the Er^{3+} content (Fig. 7), while T_m and ε_m constantly decrease (Fig. 8). In particular, the strong decrease observed for T_m appears to be coherent with the idea that Er^{3+}

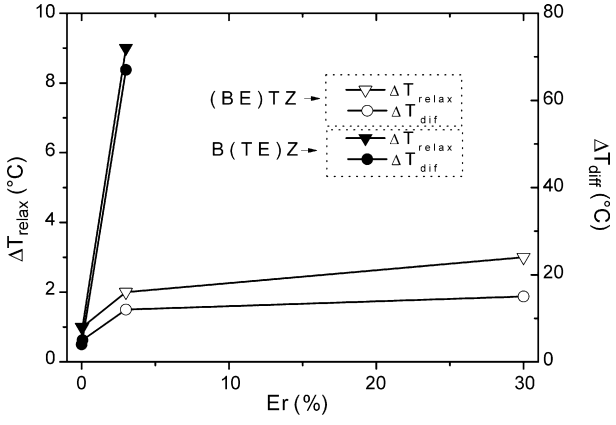

Fig. 7. Behavior of the materials' relaxation and diffuseness parameters (ΔT_{relax} and ΔT_{dif}, respectively—see text for definition) upon variation of Er^{3+} content for both (BE)TZ and B(TE)Z systems.

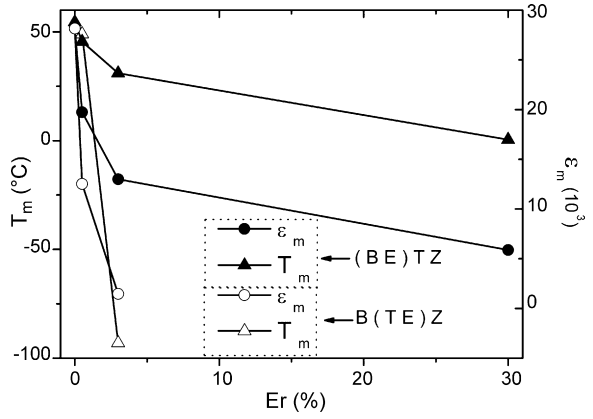

Fig. 8. Dependence of the maximum permittivity (ε_m) and phase transition temperature (T_m), processed from the 1 kHz-electrical measurements, upon variation of Er^{3+} content for both (BE)TZ and B(TE)Z systems.

incorporates at the $(Ti,Zr)^{4+}$ instead of the Ba^{2+} lattice sites for which variations of T_m would seemingly be comparatively smaller, according to observation on specifically Er^{3+}-doped $BaTiO_3$.[7] When dealing with the (BE)TZ formulated system, all the above increasing (for ΔT_{dif} and ΔT_{relax}) and decreasing (for T_m and ε_m) behaviors are drastically reduced, especially from $x = 0.03$ above, where the variations become relatively irrelevant (Figs. 7 and 8). These behaviors reproduce well the above observation according to which, for the (BE)TZ system, the solubility limit of Er^{3+} into $Ba(Ti_{0.85}Zr_{0.15})O_3$ locates close to $x = 0.03$. Difference in the magnitude of all these parameters between the (BE)TZ and B(TE)Z systems (for which a preferential substitution of Er^{3+} for the B sites is postulated in both cases) in the $0 \le x \le 0.03$ composition range, as well as the non-total stabilization of these parameters for $0.03 \le x \le 0.30$ for the (BE)TZ system, should seemingly involve the continuous introduction of Ba^{2+} vacancies (V''_{Ba}) programmed to be nominally, but unsuccessfully in practice, filled out by Er^{3+} in the (BE)TZ system (as pointed out and discussed above), combined with the presence of the pyroclore phase from about $x = 0.03$ to above (especially here for the ε_m data). We would like to however point out that, considering the complexity of the problem of amphoteric dopants, determination of substitution site and corresponding solubility limit in $BaTiO_3$[5–7,13] (provided the many probable reaction mechanisms (2.1)–(2.5) that may be involved), partial substitution of Er^{3+} for Ba^{2+} (irrespective of any preference for Ti^{4+}, when applying), should not be straightforwardly excluded, of course. Nevertheless, no clear evidence that could allow us to directly support this possibility was found in the present work.

4. Conclusions

Ceramics of Er^{3+}-doped $BaTi_{0.85}Zr_{0.15}O_3$ have been studied in this work. When prepared so as to nominally substitute for Ba^{2+} (donor-type mechanism), Er^{3+} was found to preferably incorporate at the $(Ti,Zr)^{4+}$ lattice sites, forming an insulating $Ba(Ti,Zr,Er)O_{3-\delta}$-like compound. This preference appears here to mainly or, at least, partially involve stress energy effects from

the ion size mismatch between dopant and host cations. For the finally acceptor-type solid solutions so synthesized, the solubility limit of Er^{3+} located below but close to 3 cat.%, while the formation of a pyroclore $Er_2Ti_2O_7$-based phase was detected with a further increase of the Er^{3+} content. Solubility limit and second phase formation effects, as well as departure from the invariable-like behavior expected for the electrical properties above the solubility limit, appear to arise from the Ba^{2+} vacancies (V''_{Ba}) introduced in the system to be nominally, but unsuccessfully in practice, filled out by Er^{3+}, considering that samples originally formulated and prepared so as Er^{3+} to nominally substitute for Ti^{4+} did not show such effects. Moreover, Er^{3+} was seen to inhibit the materials' grain growth process, besides promoting a change of the nature of the ferroelectric-to-paraelectric phase transition from normal-like to diffuse- and relaxor-like.

Acknowledgments

The authors acknowledge support from FAPESP and CNPq, two Brazilian funding agencies.

References

1. Moulson, A. J. and Herbert, J. M., *Electroceramics: materials, properties and applications*. Chapman-Hall, London, 1990.
2. Dobal, P. S., Dixit, A., Katiyar, R. S., Yu, Z., Guo, R. and Bhalla, A. S., Micro-Raman scattering and dielectric investigations of phase transition behavior in the $BaTiO_3$-$BaZrO_3$ system. *J Appl Phys*, 2001, **89**, 8085–8091.
3. Yu, Z., Ang, C., Guo, R. and Bhalla, A. S., Dielectric properties and high tunability of $Ba(Ti_{0.7}Zr_{0.3})O_3$ ceramics under dc electric field. *Appl Phys Lett*, 2002, **81**, 1285–1287.
4. Antonelli, E., Silva, R. S. and Hernandes, A. C., $Ba(Ti_{1-x}Zr_x)O_3$ ($x = 0{,}05$ and 0,08) ceramics obtained from nanometric powders: ferroelectric and dielectric properties. *Ferroelectrics*, 2006, **75**, 351–358.
5. Tsur, Y., Dunbar, T. D. and Randall, C. A., Crystal and defect chemistry of rare earth cations in $BaTiO_3$. *J Electroceram*, 2001, **7**, 25–34.
6. Buscaglia, M. T., Viviani, M., Buscaglia, V., Bottino, C. and Nanni, P., Incorporation of Er^{3+} into $BaTiO_3$. *J Am Ceram Soc*, 2002, **85**, 1569–1575.
7. Hwang, J. H. and Han, Y. H., Dielectrical properties of erbium doped barium titanate. *Jpn J Appl Phys*, 2001, **40**, 676–679.
8. Reddy, S. B., Rao, M. S. R. and Rao, K. P., Observation of high permittivity in Ho substituted $BaZr_{0.1}Ti_{0.9}O_3$ ceramics. *Appl Phys Lett*, 2007, **91**, 022917.
9. Shan, D., Qu, Y. F. and Song, J. J., Dielectric properties and substitution preference of yttrium doped barium zirconium titanate ceramics. *Solid State Commun*, 2007, **141**, 65–68.
10. Shannon, R. D., Revised effective ionic-radii and systematic studies of interatomic distances in halides and chalcogenides. *Acta Crystallogr A*, 1976, **32**, 751–767.
11. Lin, T.-F., Hu, C.-T. and Lin, I.-N., Influence of stoichiometry on the microstructure and positive temperature-coeficient of resistivity of semiconducting barium-tatanate ceramics. *J Am Ceram Soc*, 1990, **73**, 531–536.
12. Yu, Z., Ang, C., Guo, R. and Bhalla, A. S., Ferroelectric-relaxor behavior of $Ba(Ti_{0.7}Zr_{0.3})O_3$ ceramics. *J Appl Phys*, 2002, **92**, 2655–2657.
13. Makovec, D., Samardzija, Z. and Drofenik, M., Solid solubility of holmium, yttrium, and dysprosium in $BaTiO_3$. *J Am Ceram Soc*, 2004, **87**, 1324–1329.